To access the final edited and published work see:
https://doi.org/10.1109/TEMC.2024.3510390

Design of a LISN for Low-Frequency Conducted Emissions Measurement

Lu Wan, *Member, IEEE,* Arun D. Khilnani, *Member, IEEE,* Xinglong Wu, *Senior Member, IEEE,* Xiaokang Liu, *Senior Member, IEEE,* Sergio A. Pignari, *Fellow, IEEE,* David W.P. Thomas, *Senior Member, IEEE,* Mark Sumner, *Senior Member, IEEE,* and Flavia Grassi, *Senior Member, IEEE*

***Abstract*—In this paper, a line impedance stabilization network (LISN) with frequency bandwidth extended down to 2 kHz is designed, to address low-frequency measurement not currently aligned by the IEC and CISPR standards. For instance, different evaluation methods and limits are defined for the frequency range from 2 to 150 kHz in IEC 61000-4-7, IEC 61000-4-30, and CISPR 16-2-1. To this end, the limitations of existing LISNs for conducted emission (CE) measurement are firstly investigated, and a two-stage cascaded filter LISN topology is designed by resorting to multi-objective optimization. To ensure the desired performance, the influence of component tolerance and parasitic effects are studied. Eventually, a LISN prototype was manufactured and characterized. It was proven that the proposed LISN assures improved performance in terms of decoupling factor (DF), voltage division factor (VDF), and LISN impedance in the frequency interval starting from 2 kHz.**

***Index Terms*—Conducted emission, line impedance stabilization network (LISN), low frequency, multi-objective optimization.**

I. Introduction

THE widespread use of power electronics devices with switching frequency of a few kilohertz (kHz), poses the challenge of evaluating the conducted emissions (CEs) exiting these devices in the low-frequency interval from 2 kHz up to 150 kHz, which is not currently covered by all EMC standards [1]. Several electromagnetic interference (EMI) attributed to noise between 2 to 150 kHz have been documented in [2], such as malfunctioning in wind farms caused by defective generators and abnormal meter readings in PV farms. In particular, low-frequency disturbances exiting power converters can lead to coexistence issues between power and data transmission, mainly because narrowband power line communication (PLC) systems partially exploit this frequency range (such as 3 to 95 kHz for CENELEC Band A [3]). However, neither power quality nor EMC standards fully address this frequency range. As outlined in [4], [5], the methodologies for CE evaluation foreseen by the current IEC and CISPR standards only partially cover the range from 2 to 150 kHz. Specifically, IEC 61000-4-7 and IEC 61000-4-30 prescribe different approaches for CE evaluation in the frequency range from 2 to 9 kHz, and the range of 9 to 150 kHz, respectively. These two IEC standards differ from the evaluation method defined in CISPR 16-2-1, where only the frequency range above 9 kHz is considered. Hence, the various evaluation methodologies may lead to inconsistent results, thus requiring an alignment.

To ensure reproducible measurements, the CE exiting the device under test (DUT) is to be measured using a stable and well-defined impedance. To this end, the use of a line impedance stabilization network (LISN) is foreseen, which also performs the following functions. First, the LISN acts as a low-pass filter (LPF) allowing the transfer of AC or DC mains power to the DUT. Second, it couples the CE generated by the DUT to the receiver port. Third, it assures decoupling between the mains and the receiver/DUT port, preventing the noise from the mains to be measured by the receiver.

However, since the bandwidths of existing LISNs start from 9 kHz or 150 kHz, according to the standard CISPR 16-1-2 [6], the above LISN functions may not be guaranteed in the whole frequency range from 2 kHz up to 150 kHz.

Some literature addresses challenges and techniques for LISN design. For instance, in [7] a multistage LISN operating from 150 kHz was proposed to ensure the requirement in the Standard AIAA (S-121A-2017). In [8], a miniaturized laboratory LISN was designed and characterized up to 100 MHz for pre-compliance measurements. In [9] computer-controlled LISNs with automated test procedures were developed for CISPR 16-1-2 Band B. Some studies modified the receiver ports of LISNs for CISPR 16-1-2 Band A, enabling simultaneous measurement of phase voltages and common mode (CM) and differential mode (DM) components [10]. However, none of these studies specifically focused on the frequency band below 9 kHz.

If standard LISNs were employed to measure CE from 2 to 150 kHz, additional filters would be required to enhance the LISN performance. For instance, in [11] the conventional configuration of CE measurement using a CISPR 16-1-2 LISN (for Band A) was augmented with a high-pass filter (HPF) and LPF attached to the LISNs' radio frequency (RF) port. However, the behavior of this augmented test setup at low frequencies should be evaluated thoroughly. A theoretical design of a DC LISN in [12] did not consider formulating

This project has received funding from the European Union's Horizon 2020 research and innovation programme under the Marie-Skłodowska-Curie grant agreement No 812753 and No 955646. (*Corresponding author: Lu Wan)*

L. Wan is with Hitachi Energy Research, Baden-Dättwil, 5405, Switzerland (e-mail:lu.wan@hitachienergy.com).

A. D. Khilnani, D.W.P. Thomas, and M. Sumner are with the Department of Electrical and Electronic Engineering, University of Nottingham, Nottingham, NG7 2RD, UK (e-mail:arun.khilnani1@nottingham.ac.uk; david.thomas1@nottingham.ac.uk; mark.sumner@nottingham.ac.uk).

X. Wu, X. Liu, F. Grassi, and S.A. Pignari are with the Department of Electronics, Information and Bioengineering, Politecnico di Milano, Milan, 20133, Italy (e-mail:xinglong.wu@polimi.it; xiaokang.liu@polimi.it; flavia.grassi@polimi.it; sergio.pignari@polimi.it).

LISN performance in the design methodology and it was not experimentally verified. In conclusion, to the best of the authors' knowledge, LISNs targeted at low frequencies are commercially unavailable, and there is scarce research on this particular topic in the literature.

This study aims to identify the limitations in existing LISNs for low-frequency CE measurement and propose a new LISN design. The proposed LISN primarily focuses on enhancing its performance at low frequencies (starting from 2 kHz) that is not covered by any existing LISNs, while maintaining its functionality up to 30 MHz. To this end, three limitations in terms of decoupling factor (DF), voltage division factor (VDF), and LISN impedance of the standard LISN for low-frequency CE measurement are addressed. To overcome these limitations, a versatile LISN design procedure incorporating multi-objective optimization (MOO) is proposed to design and optimize the parameters of a two-stage LISN topology. Several aspects are considered to ensure the desired behavior of the designed LISN, including the sensitivity to component tolerance and the influence of parasitic effects. Eventually, a LISN prototype is fabricated and characterized.

The manuscript is organized as follows. Section II investigates the limitations of existing LISN for low-frequency CE measurement. Section III proposes the design procedure for the LISN. The considerations for selecting resistors and capacitors, as well as designing inductors, are discussed in Section IV. Section V provides an equivalent circuit model of the constructed LISN prototype to investigate parasitic effects. Additionally, the LISN characteristics are measured. Finally, Section VI summarizes this work.

II. Limitations of Existing LISNs

Depending on the specific DUT and the frequency range of interest, different LISN topologies are defined in various standards (CISPR 16, CISPR 25, MIL-STD 461/462, ANSIC 63.4, ISO 7637-2, DO 160G, etc.). A common type is the V-LISN, which measures the voltage between phases and ground, also called unsymmetric disturbance. Without loss of generality, to illustrate the limitations, we will consider two types of V-LISN with different LISN impedances defined in CISPR 16 and CISPR 25. The AC LISN defined in CISPR 16, equipped with a 50 μH inductor, is often employed to evaluate equipment like inverters and EV charges connected to 50 Hz (or 60 Hz) power supplies. On the other hand, the automotive LISN (defined in CISPR 25), equipped with a 5 μH inductor, is typically used to assess equipment for automotive, vehicles, boats, and aircraft, which are connected to onboard DC or 400 Hz power mains. This Section investigates the limitations of both AC and automotive LISN, whose topologies specified in CISPR 16 and CISPR 25 are shown in Fig. 1.

A. Variability of LISN Impedance

The AC LISN topology see [Fig. 1(a)] is utilized for Band A (from 9 to 150 kHz), with impedance defined as (50 μH + 5 Ω) $\|$ 50 Ω and illustrated as Standard (Std.) Band A in Fig. 2(a). This topology typically satisfies the impedance requirement for Band B (from 150 kHz to 30 MHz) (50 μH $\|$ 50 Ω as

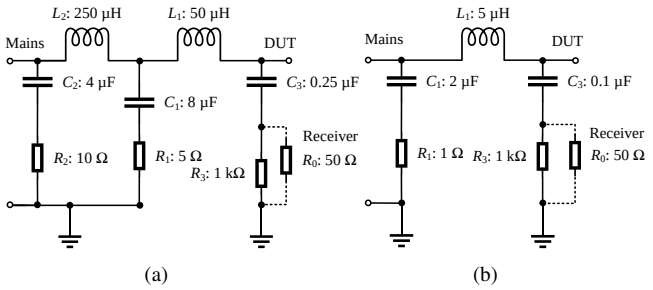

Fig. 1. LISN topologies specified in (a) CISPR 16, AC LISN: (50 μH + 5 Ω) $\|$ 50 Ω and (b) CISPR 25, automotive LISN: (5 μH + 1 Ω) $\|$ 50 Ω, the notation '$\|$' represents two impedances in parallel.

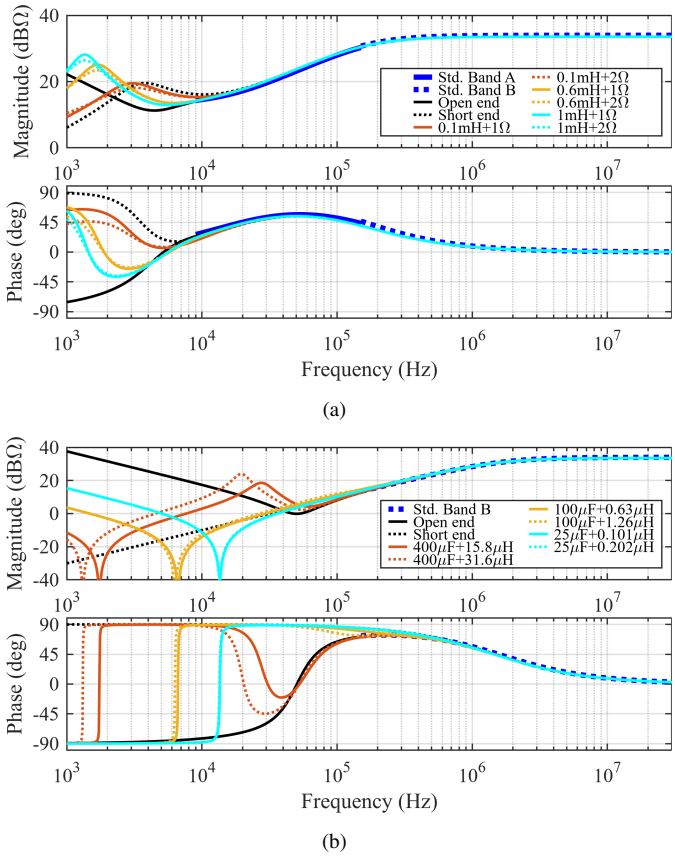

Fig. 2. Impedance of the (a) AC LISN and (b) automotive LISN for different values of the main impedance.

Std. Band B in Fig. 2(a)). Consequently, the AC LISN can be employed for the frequency range from 9 kHz to 30 MHz. CISPR 16-1-2 allows a 20% tolerance for the magnitude and $\pm$ 11.5° for the phase of the LISN impedance. However, if the impedance of the AC power supply (typically assumed to be inductive) fluctuates, the overall impedance seen by DUT may exhibit significant variations below 9 kHz, as depicted in Fig. 2(a), where different mains impedances are considered.

Similarly, the automotive LISN topology depicted in Fig. 1(b) is intended for Bands B and C (from 150 kHz to 108 MHz), whose impedance is defined as (5 μH + 1 Ω) $\|$ 50 Ω. However, when power converters are employed as a power supply, whose output impedance is commonly capacitive at low frequencies, the automotive LISN cannot provide stable

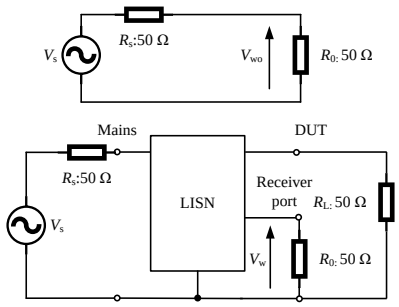

Fig. 3. Definition of the LISN decoupling factor according to CISPR 16-1-2 by two measurement setups.

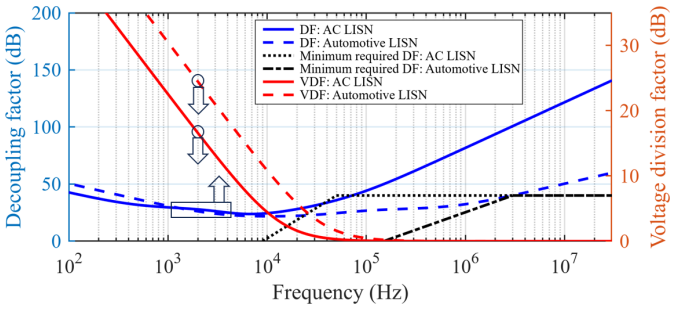

Fig. 4. DF (left axis) and VDF (right axis) of both AC and automotive LISNs.

impedance below 150 kHz. This is shown in Fig. 2(b), where, for simplicity, the LISN impedance between phase and ground was considered. However, similar conclusions can be drawn also for the line-to-line impedance, with consequent issues in terms of measurement repeatability at low frequency.

B. Decoupling Factor and Voltage Division Factor

Other limitations are associated with two parameters defined in CISPR 16-1-2, that is the decoupling factor and the voltage division factor. The DF represents the level of isolation (or insertion loss) between each mains phase and the corresponding RF receiver port of the LISN, considering the specific source (R_s) and load impedances (R_L) at the mains and DUT port (specified as 50 Ω resistors in CISPR 16-1-2, as shown in Fig. 3). With reference to the measurement setup in Fig. 3, the DF is defined as: $\mathrm{DF} \triangleq V_\mathrm{wo}/V_\mathrm{w}$. The VDF is defined as the voltage ratio between the DUT port and RF receiver port, with the latter terminated by a 50 Ω load.

Fig. 4 illustrates the DF and VDF of both AC and automotive LISNs, along with their DF requirements. For instance, in CISPR 16-1-2 [6], the minimal requirement of DF for AC LISN from 9 kHz to 50 kHz increases linearly with the logarithm of frequency, and the minimal requirement is 40 dB above 50 kHz, as plotted in dot black line in Fig. 4. This comparison indicates that the DF (plotted as blue curves) for both LISNs decreases significantly below their respective bandwidths, which is insufficient to isolate the spurious signals from the mains to the RF receiver port. In addition, the VDF is dramatically higher below 9 kHz for AC LISN and 150 kHz for automotive LISN (plotted as red curves). While the measurement of VDF is required and should be compensated for the low-frequency range [6], a large VDF means that CE from the DUT port to the receiver port is attenuated significantly, which limits the accuracy of CE measurement at low frequencies. As outlined in Fig. 4, an increase in DF and a decrease in VDF are needed in order to improve the LISN performance at low frequency.

The aforementioned limitations are further assessed in the CE measurement setup of a three-phase PV-inverter system in [13] and the cascaded boost converter in [12]. The study reveals that the unstable LISN impedances lead to a varying evaluated CE level. Besides, due to insufficient DF, spurious interferences from the mains can pollute the measured CEs [13].

III. Low-Frequency LISN Design

To enhance the low-frequency performance of the existing AC LISN, an augmented solution was proposed in [13]. However, this solution requires modifying the adapters and connectors of each port, with efforts comparable to building an entirely LISN. Therefore, this Section presents a design methodology based on a multi-objective optimization algorithm to design a LISN with bandwidth from 2 kHz to 30 MHz.

A. LISN Topology

A basic V-LISN topology (such as the automotive LISN depicted in Fig. 1(b)) includes an LPF (L_1, C_1, and R_1) between the mains and DUT, and an HPF (C_3 and R_3) between the DUT and receiver port. The LPF filters out high-frequency noise originating from the power utility and provides a path for DC or AC power to reach the DUT. The HPF creates the CE coupling path from the DUT to the RF receiver port, meanwhile blocking low-frequency noise components. To meet the requirements of Band A, an additional LPF stage is incorporated to extend the frequency range, in order to have a bandwidth starting from 9 kHz instead of 150 kHz. (an example of LPF consisting of L_2, C_2, and R_2 in the case of the AC LISN is shown in Fig. 1(a)).

Intuitively, to further extend the frequency boundary from 9 kHz to 2 kHz, two approaches can be adopted: (1) create a multi-stage LISN, such as by adding additional LPF to form a three-stage LPF structure, and (2) modify the two-stage structure by properly tailoring RLC parameters for low-frequency range. The first approach was adopted in [11], [13] by adding additional filters to the standard AC LISN. However, this approach leads to a bulky LISN volume, especially for high power ratings. Besides, more stages introduce more complexity to the circuit that leads to a concern of oscillatory response and multiple peaks in DF transfer function as discussed in [7]. Therefore, the second approach to design a minimal two-stage structure is employed to develop a LISN allowing CE measurement starting from 2 kHz.

Accordingly, the LISN configuration considered in this study, shown in Fig. 5, consists of a two-stage topology, including two LPFs and one HPF. In the first stage, the

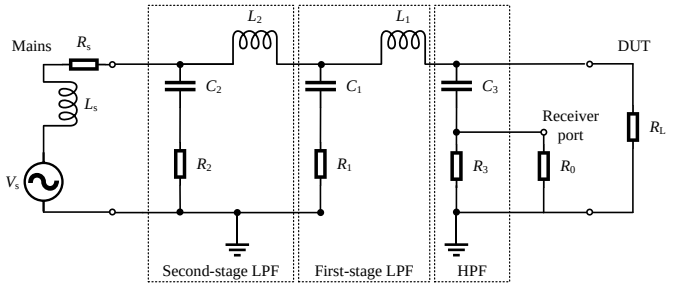

Fig. 5. Two-stage topology (with two LPFs and one HPF) of the designed LISN.

inductor L_1 emulates the inductance of the power line or grid. For a wiring system on a ship or cargo aircraft, a 50 μH inductor is selected to represent the power distribution wiring running for approximately 50 meters [14]. A reduced inductance value, such as 5 μH in the automotive LISN, is recommended for smaller platforms like fighter aircraft. It should be noted that some research has shown that usually, the impedances of power distribution networks exhibit more complex responses [15]. However, to maintain consistency with the requirements of CISPR16-1-2, we will consider a 50 μH inductor (L_1), to ensure the compliance of the designed LISN with existing Standards. The nominal values of the other components in Fig. 5 will be determined using the MOO method in subsequent steps.

B. Multi-objective Optimization of LISN Parameters

To effectively estimate the RLC parameters of the three filters, a procedure based on multi-objective optimization is here adopted for a twofold reason. Firstly, the optimization allows to directly adapt the filter response to the desired LISN performance, including (1) a higher DF, (2) a lower VDF, (3) a more stable LISN impedance compared to standard AC LISNs, and (4) small LC components in LPFs. Secondly, tradeoffs may arise between the desired LISN characteristics, such as the need for smaller LC components of LPF and sufficiently higher DF at low frequencies. A tradeoff can be achieved by resorting to multi-objective optimization.

Indeed, MOO algorithms are widely applied in problems involving tradeoffs between multiple objectives. The problem is defined by formulating a set of objective functions to be minimized or maximized, considering relevant constraints. Unlike single-objective optimization, where all objectives are combined into a single function using a weighted sum, the MOO treats all objectives equally, resulting in the same number of dimensions in the Pareto front. The Pareto front is a set of points in the parameter space with non-inferior fitness objective function values. For each point on the Pareto front, one objective can be improved only by degrading other objectives. Thus, evaluating the relationship and possible tradeoffs among all objectives is achievable with multi-objective optimization. The final solution, represented by a variable vector, is determined by assessing the chosen evaluation functions on the Pareto front [16].

Specifically for the case of LISN design, the LISN features (i.e., DF, VDF, impedance, and LC components in LPFs) are formulated as several objective functions to be optimized under certain constraints. Eventually, the final solution is determined by evaluating the obtained parameter space. Among available MOO algorithms, we employ a genetic algorithm to find non-inferior solutions within the Pareto front by the Matlab Optimization Toolbox [17].

TABLE I
THE LOWER AND UPPER BOUNDS OF VARIABLES

$\boldsymbol{x}$	C_2 (μF)	R_2 (Ω)	L_2 (μH)	C_1 (μF)	R_1 (Ω)	C_3 (μF)	R_3 (Ω)
$\boldsymbol{lb}$	4	1	250	8	1	0.25	1k
$\boldsymbol{ub}$	40	100	800	80	100	50	100k

The MOO workflow for designing the functional parameters of the proposed LISN can be summarized as follows:

1) Define the variable vector $\boldsymbol{x}$ to represent the unknown parameters.
2) Establish the lower and upper bounds ($\boldsymbol{lb}$, $\boldsymbol{ub}$) for the variable vector based on practical considerations.
3) Analytically formulate the LISN behavior as a minimization problem using the objective function vector $\boldsymbol{f}(\boldsymbol{x})$.
4) Set the desired LISN specifications through nonlinear constraints ($\boldsymbol{nc}$).
5) Apply the MOO algorithm to identify the feasible solution space by minimizing the objective vector $\boldsymbol{f}(\boldsymbol{x})$, while satisfying the bounds ($\boldsymbol{lb}$, $\boldsymbol{ub}$) and nonlinear constraints ($\boldsymbol{nc}$).
6) Determine the final solution by evaluating the value of the evaluation function $\boldsymbol{E_v}(\boldsymbol{x})$.

A detailed explanation of each step will be provided in the following.

First of all, the variable vector $\boldsymbol{x}$ is defined by collecting all the parameters in Fig. 5, with the only exception of inductance L_1, which was set equal to 50 μH, as previously explained, that is:

$$\boldsymbol{x} = \left[\begin{array}{ccccccc} C_2 & R_2 & L_2 & C_1 & R_1 & C_3 & R_3 \end{array} \right] \qquad (1)$$

To ensure a practical solution region, suitable bounds for the variable vector should be assigned. As a first constraint, we restrict the upper limit of capacitors C_1 and C_2 to be ten times larger than their lower bounds to restrain the leakage current to ground. Also, the upper bound to the inductance L_2 is set to 800 μH, to mitigate the effects of self-resonant frequency (SRF) in large inductors, which can occur at lower frequencies. The upper bounds of resistors are set one hundred times larger than their lower bounds. The lower bounds of the variable LC are set equal to the values of the parameters of the standard AC LISN (see Table I). The impact of the SRF of LC components on the LISN behavior along with considerations for their selection/design will be discussed in Section IV.

The core part of formulating a MOO problem is to define objectives and (nonlinear) constraints. In general, all desired LISN features (in terms of the DF, VDF, impedance, and LC components) could be set as objective functions and/or constraints. However, objectives and constraints have different

functionality and influence on the final MOO solution. Specifically, each objective creates one dimension in the Pareto front, where the parameter space must satisfy the set constraints. Therefore, several aspects should be considered when defining the objectives and constraints: (1) It is recommended to set the feature as a constraint if it is regarded as a priority and compulsory requirement with well-defined limits. (2) Features with potential tradeoffs but without explicit requirements should be set as objectives. In this work, five objectives are set to evaluate the DF, VDF, and LC components, and two nonlinear constraints are set for LISN impedance and DF. The definitions of objectives and constraints are explained in detail as follows.

The first objective function is defined as the maximum value of 1/DF in the frequency interval from 50 Hz to 2 kHz, so to reduce the influence of the harmonics of the 50 Hz component at mains. Since the limit of this quantity is not defined in the standard, setting it as an objective rather than as a constraint is preferable. The second function is set as the VDF at 2 kHz, since VDF has the highest value at 2 kHz in the frequency range of interest. According to the standard, the VDF should be measured and compensated before measuring CEs, which indicates that setting an objective is more suitable than a constraint. Besides, the variables C_1, C_2, and L_2 are also employed as objective functions, aiming to minimize their values. Therefore, the objective function vector is formulated as follows:

$$\boldsymbol{f}(\boldsymbol{x}) = \left[\begin{array}{cccc} \max\limits_{50\text{Hz}-2\text{kHz}} \left\{ \frac{1}{\text{DF}} \right\} & \text{VDF}_{2\text{kHz}} & C_2 & L_2 & C_1 \end{array} \right] \tag{2}$$

where the analytical expressions of DF and VDF, which are omitted here for brevity, are function of the unknown RLC parameters in Fig. 5. These expressions can be derived based on the definition of DF and VDF in CISPR 16-1-2 and the circuit in Fig. 5.

Regarding nonlinear constraints, the variation of LISN impedance and DF margin are defined, since these two features are prioritized LISN performance and the limits can be well-defined by comparing with the standard AC LISN. The variation of LISN impedance under two extreme cases of mains impedance is restricted to 1 percent. The DF is required to have a 10 dB margin compared to the existing AC LISN. Both constraints are set for 2 kHz, as it is the lowest boundary and worst case in the frequency range of interest. The margin values can be adjusted according to future standard requirements. Eventually, the desired LISN specifications at 2 kHz are assigned in terms of LISN impedance and DF by the following nonlinear constraints:

$$\mathbf{nc}_{2\text{kHz}} = \begin{cases} \frac{||Z_\text{s}|-|Z_\text{o}||}{\min(|Z_\text{s}|,|Z_\text{o}|)} < 1\% \\ \frac{1}{\text{DF}} < \frac{1}{\text{DF}_{50\mu\text{H}}} - 10\text{dB} \end{cases} \tag{3}$$

where Z_s and Z_o represent the impedances of the proposed LISN when the side of the main is short-end and open-end, respectively. DF and $\text{DF}_{50\mu\text{H}}$ indicate the decoupling factors of the proposed LISN and the standard AC LISN, respectively. Similar to the objective functions, the expressions of LISN impedance can be analytically derived based on the definition in CISPR 16-1-2.

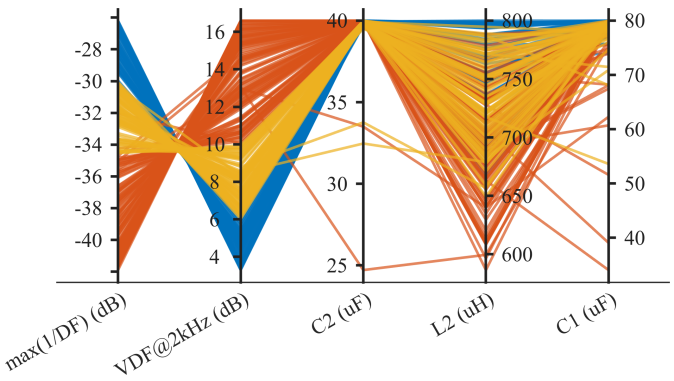

Fig. 6. Parallel plot of MOO results w.r.t. objective functions: All feasible solutions represented by polylines satisfy the upper and lower bounds ($\boldsymbol{lb}$, $\boldsymbol{ub}$) and nonlinear constraints ($\boldsymbol{nc}$).

TABLE II
TWO SOLUTIONS SCREENED BY EVALUATION FUNCTIONS AND THE FINAL SELECTED VALUES

Solution	C_2 (μF)	R_2 (Ω)	L_2 (μH)	C_1 (μF)	R_1 (Ω)	C_3 (μF)	R_3 (Ω)
1	39.97	1.88	668.05	79.15	1.0061	1.06	1.09k
2	39.91	1.86	692.13	79.82	1.0070	1.12	1.11k
Designed	40	2	670	80	1	1	1k

After applying the MOO algorithm, the feasible solutions in Fig. 6 are obtained (number of solutions is 210 when the population size of the genetic algorithm is set as 600). For the first two objectives, a trade-off between the VDF and DF is necessary. Moreover, the analysis reveals that most solutions cluster towards the upper bounds of capacitors C_1 and C_2 (see Fig. 6). Consequently, selecting larger capacitors seems to be necessary to enhance the LISN performance at low frequencies, although small capacitance values are preferable in terms of leakage current. The spread of solutions obtained for inductor L_2 suggests the possibility to exploit small inductance values.

In principle, evaluation functions could be set for all or part of the objectives. Based on the analysis in Fig. 6, one of VDF or DF is sufficient to be set as an evaluation function. Besides, because the distribution of L_2 is sparser than the distribution of capacitors, selecting L_2 as an evaluation function is preferable to selecting C_1 and C_2. Therefore, to select a suitable solution in Fig. 6, two evaluation functions are defined that is the VDF at 2 kHz and the inductance of L_2:

$$\boldsymbol{E_v}(\boldsymbol{x}) = \left[\begin{array}{cc} \text{VDF}_{2\text{kHz}} & L_2 \end{array} \right] \tag{4}$$

By enforcing the constraints $\text{VDF}_{2\text{kHz}} < 6$ dB and $L_2 < 700$ μH, the optimization leads to the two solutions shown in Table II, which provide similar RLC values except for inductance L_2. This inductor can be selected in the range from 668 to 692 μH. Therefore, the values are rounded based on the first solution in Table II leading to: C_2 = 40 μF, R_2 = 2 Ω, L_2 = 670 μH, C_1 = 80 μF, R_1 = 1 Ω, C_3 = 1 μF, and R_3 = 1 kΩ.

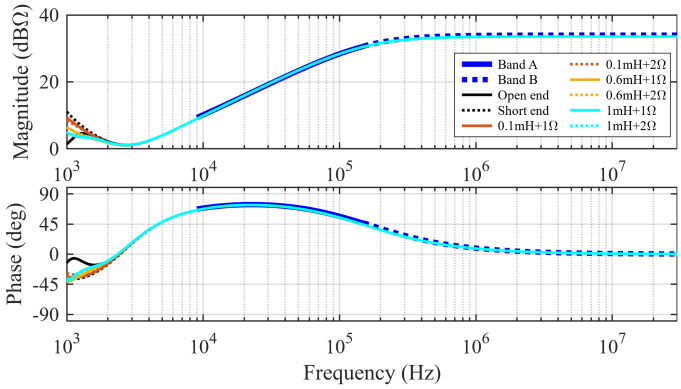

(a)

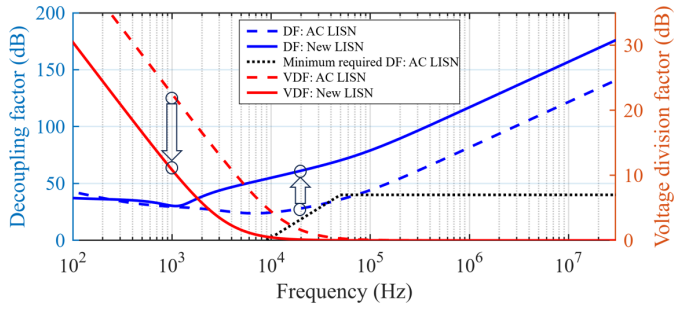

(b)

Fig. 7. Theoretical characteristics of the proposed LISN: (a) impedance under different conditions of mains and (b) DF (left axis) and VDF (right axis) compared with the standard AC LISN.

TABLE III
THEORETICAL IMPEDANCE, DF AND VDF OF THE TWO LISNS AT 2 KHZ

features @2kHz		Standard AC LISN	Proposed AC LISN
LISN impedance	magnitude deviation (%)	33.0	0.6
	phase shift (deg)	141.0	5.8
DF (dB)		27.8	38.4
VDF (dB)		16.6	5.8

C. Theoretical Performance of the Proposed LISN

The impedance of the proposed LISN is plotted in Fig. 7(a) for different values of the main impedance. Above 2 kHz, the proposed LISN exhibits a more stable impedance compared to the standard AC LISN (see Fig. 2(a)). Fig. 7(b) compares the DF and VDF of the two LISNs, and reveals a significant improvement for both the two parameters (i.e., a significant increase of DF, and a decrease of the VDF). Such an improvement can be further appreciated in Table III, where values for these parameters at 2 kHz are compared.

Although the theoretical performance of the proposed LISN looks promising, possible limitations due to tolerances and non-ideal behavior of the involved components have to be carefully evaluated and taken into account for the practical realization of the LISN prototype.

IV. SELECTION OF RLC COMPONENTS

A. Sensitivity to Component Tolerences

In order to select RLC components with acceptable tolerance, in this Section a sensitivity analysis is carried out to

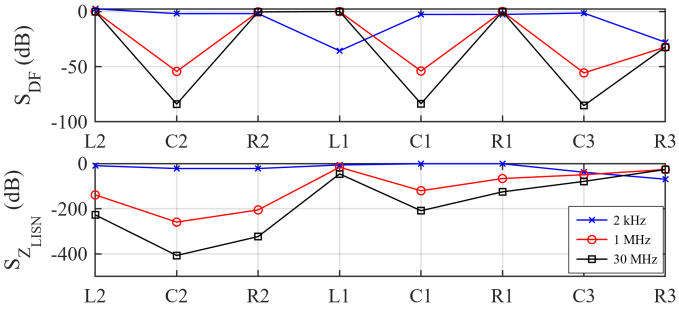

Fig. 8. Sensitivity coefficient of DF (top panel) and Z_{LISN} (bottom panel).

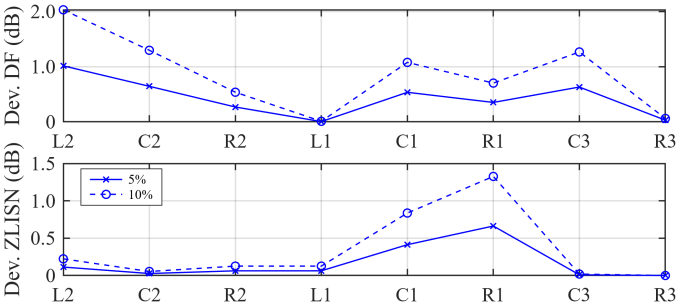

Fig. 9. Deviation of DF (top panel) and Z_{LISN} (bottom panel) under 5% and 10% tolerance of RLC components at 2 kHz.

estimate the influence of the exploited RLC components on the expected LISN performance. To this end, the derivative-based local sensitivity analysis is applied, which allows estimating the influence of the variability of a single component while the others are set to their nominal values. Accordingly, the sensitivity coefficient associated with the LISN impedance and DF is cast in normalized form as:

$$s_x^y = \frac{\partial y/y}{\partial x/x} \tag{5}$$

where y represents DF or Z_{LISN}, and x denotes the tolerance of the value of the RLC component under analysis.

Fig. 8 illustrates the sensitivity coefficients of DF and Z_{LISN} at 2 kHz, 1 MHz, and 30 MHz. As far as the DF is concerned, it is observed that L_2, R_2, and R_1 consistently play a significant role both at high and low frequency. Conversely, the capacitors (C_1, C_2, and C_3) demonstrate greater significance at low frequencies, which suggests the need for selecting components with smaller tolerance in order to ensure low-frequency performance. Concerning Z_{LISN}, the 50 μH inductor L_1 influences the impedance response regardless of frequency. However, at low frequencies, also the tolerance of other components (L_2, C_2, R_2, C_1, and R_1) may significantly influence the frequency response, as expected from Section II-A.

To select components with appropriate tolerances, the expected deviations of DF and Z_{LISN} at 2 kHz values are estimated, by assuming a 5% and 10% tolerance of RLC component values (see Fig. 9). The results show that a 10% tolerance for R_2, L_1, and R_3 is acceptable. However, to achieve less deviation in the desired LISN behavior at low frequencies, a 5% tolerance is recommended for the remaining

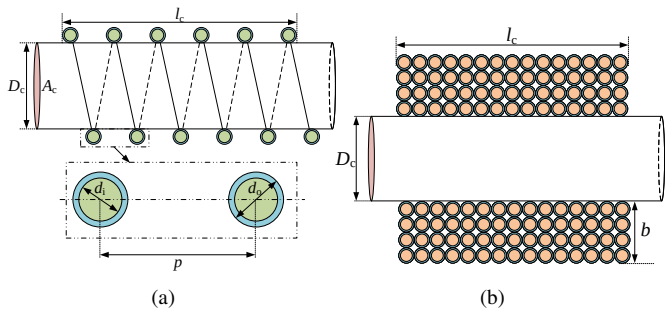

(a) (b)

Fig. 10. Wire arrangements of (a) single-layer air-core inductor for 50 μH L_1 and (b) multi-layer air-core inductor for 670 μH L_2.

TABLE IV
SPECIFICATIONS OF TWO AD HOC INDUCTORS IN THE PROPOSED LISN

Parameter	**50 μH inductor L_1**	**670 μH inductor L_2**
d_i (mm)	2.65	
d_o (mm)	2.70	
p (mm)	average: 5.38	/
D_c (mm)	103.2	150
N	33	51 from bottom to top: 9-8-8-8-8-8-2
l_c (mm)	175	25
L (μH)	51.5	666.6
C_tot (pF)	1.4	74.1
SRF (MHz)	18.5	0.7

parameters. Therefore, resistors and capacitors with a 5% tolerance were procured, whereas ad hoc inductors were designed and manufactured in order to assure the expected performance, as will be detailed in the next Section.

B. Inductors Design

Several factors were considered when designing the inductors for the LISN prototype. First, air-core inductors are exploited to avoid saturation. Second, to ensure the desired behavior of the LISN at high frequencies, inductors with small stray capacitances (and large SRF) are required. Additionally, it has to be considered that the size of inductors is limited by volume constraints of the LISN prototype.

The 50 μH inductor L_1 and 670 μH inductor L_2 are constructed as single-layer and multi-layer air-core types, respectively, as shown in Fig. 10.

For the single-layer air-core inductor, the inductance L_1 and stray capacitances C_stray can be computed by (6) [18] and the empirical expression (7) [19], respectively:

$$L_1 = \frac{\mu_0 A_\mathrm{c} N^2}{l_\mathrm{c} \mathrm{K}} \tag{6}$$

$$C_\mathrm{stray} = \frac{4\varepsilon_0 l_\mathrm{c}}{\pi}\left\{0.18\frac{D_\mathrm{c}}{l_\mathrm{c}} + 0.25 + 0.6\left(\frac{D_\mathrm{c}}{l_\mathrm{c}}\right)^{1.5}\right\} \tag{7}$$

where μ_0 denotes the free space permeability. N is the number of turns. D_c is the bobin diameter. $A_\mathrm{c} = \pi\left(D_\mathrm{c}/2\right)^2$ represents the cross-sectional area of the bobbin. $l_c = (N-1)\,p + d_o$ is the length of the inductor. $\mathrm{K} = 1 + 0.9D_c/(2l_c)$ is the Nagaoka's coefficient [18] and ε_0 denotes the vacuum permittivity.

For the multi-layer air-core inductor, the inductance can be calculated by the empirical expression [20]:

$$L_2 = \frac{31.6N^2r^2}{6r + 9l_c + 10b} \times 10^{-6} \tag{8}$$

where, $r = D_\mathrm{c}/2$ is the radius of the bobbin, l_c is the length of the inductor, and b is the width of total layers.

The stray capacitances of the multi-layer air-core inductor are computed using an enhanced analytical model based on the energy-conservation method not reported here for the sake of brevity [21]. Table IV presents the final design, as well as the measured inductance and stray capacitances for the two inductors.

V. VALIDATION OF THE PROPOSED LISN DESIGN

This Section is aimed at assess the feasibility of the proposed LISN design. To this end, as the first step, we investigate the impact of parasitic on the LISN theoretical performance, by the use of a suitable circuit model, whose parameters are obtained by fitting measurement data. Then, the actual performance of the designed LISN will be evaluated by experimental measurement carried out on a LISN prototype fabricated in the Power Electronics and Machines Control Department at the University of Nottingham.

A. LISN Circuit Model Including Parasitics

To investigate the actual LISN performance, a circuit model involving parasitics is developed. To this end, all LC components are measured using an impedance analyzer (Keysight E4990A) in the frequency interval from 20 Hz to 100 MHz (refer to Fig. 11(a)). Since the objective is to verify the influence of parasitics on the LISN frequency response, the involved capacitors are represented as the series connection of a nominal capacitor C, an equivalent series resistor (ESR), and an equivalent series inductor (ESL). The inductors are modeled using a nominal inductance L, an ESR, an equivalent parallel capacitor (EPC), and an equivalent parallel resistor (EPR). The circuit parameters for LC components based on fitting the measured impedances are collected in Table V. The resistors should be modeled by a nominal resistance R, equivalent parallel capacitor (EPC), and ESL for more accurate results. Since the measured impedances of resistors exhibit resistive behavior up to 30 MHz, they are regarded as ideal resistors.

The LISN impedance obtained by the measurement-based circuit model is compared versus the theoretical LISN impedance in Fig. 12(a). The comparison shows that the actual LISN impedance exhibits a resonance at approximately 17 MHz, which is consistent with the self-resonant frequency of the 50 μH inductor L_1. This observation confirms that the parasitic effects of inductor L_1 have a significant impact on the LISN impedance, corroborating the results of the sensitivity analysis presented in Section IV-A.

The comparison in terms of theoretical and actual DF is shown in Fig. 12(b), which reveals a significant impact of parasitics on the LISN DF. Specifically, the inductors L_1 and L_2 introduce two poles at their respective SRF (indicated by

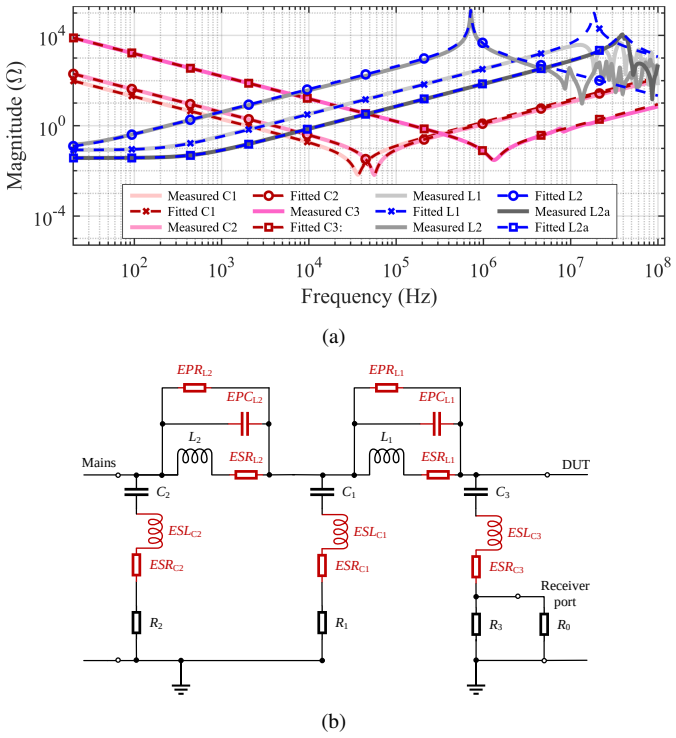

Fig. 11. (a) Impedance magnitude of LC components: measured by impedance analyzer vs fitted circuit model; (b) LISN circuit model including parasitics.

TABLE V
VALUES OF LC CIRCUIT MODEL EXTRACTED FROM MEASUREMENT

Element	Nominal value	Parameter of fitted circuit model
C_1	80 μF	C_1=81.8 μF, $\mathrm{ESR_{C1}}$=6.7 mΩ $\mathrm{ESL_{C1}}$=231.6 nH, $\mathrm{SRF_{C1}}$=36.6 kHz
C_2	40 μF	C_2=40.1 μF, $\mathrm{ESR_{C2}}$=6.5 mΩ $\mathrm{ESL_{C2}}$=200.1 nH, $\mathrm{SRF_{C2}}$=56.2 kHz
C_3	1 μF	C_3=1.0 μF, $\mathrm{ESR_{C3}}$=30.0 mΩ $\mathrm{ESL_{C3}}$=14.2 nH, $\mathrm{SRF_{C3}}$=1.3 MHz
L_1	50 μH	L_1=51.5 μH, $\mathrm{ESR_{L1}}$=84.1 mΩ $\mathrm{EPR_{L1}}$=100 kΩ, $\mathrm{EPC_{L1}}$=1.4 pF $\mathrm{SRF_{L1}}$=18.5 MHz
L_2	670 μH	L_2=666.6 μH, $\mathrm{ESR_{L2}}$=91.8 mΩ $\mathrm{EPR_{L2}}$=131.3 kΩ, $\mathrm{EPC_{L2}}$=74.1 pF $\mathrm{SRF_{L2}}$=716.3 kHz
L_{2a}	10 μH	L_{2a}=11.6 μH, $\mathrm{ESR_{L2a}}$=31.9 mΩ $\mathrm{EPR_{L2a}}$=11.1 kΩ, $\mathrm{EPC_{L2a}}$=1.4 pF $\mathrm{SRF_{L2a}}$=39.1 MHz

the two dashed curves in Fig. 12(b)). The parasitic effects caused by the capacitors maintain the DF at a flat level of approximately 120 dB (represented by the yellow curve). The combined influence of capacitors and inductors can decrease the DF below 40 dB (see the black curve). Therefore, increasing the SRF of both inductors can improve the DF at high frequencies.

A possible solution to increase the inductor SRF is to sectionalize the windings of the inductors. Specifically, each section, consisting of multiple turns, is shunted by a resistor. This winding configuration helps damping internal resonances within the inductor. In this study, however, a different solution was adopted. Namely, an additional 10 μH inductor L_{2a} is connected in series with the 670 μH inductor L_2. The inductance L_{2a}, to reach the values in the second solution

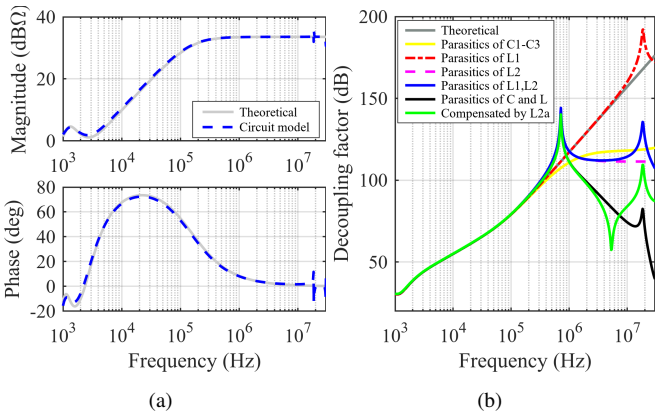

Fig. 12. Comparison of the LISN theoretical performance versus those predicted by circuit model involving parasitic (a) impedance and (b) DF.

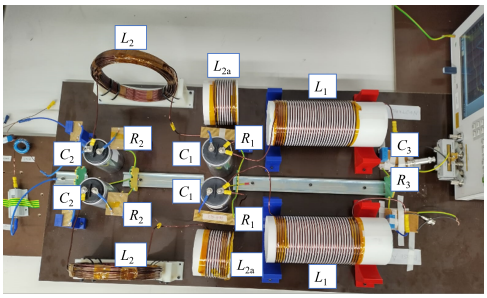

Fig. 13. LISN prototype and setup for LISN impedance measurement.

in Table II, can be selected up to 22 μH. Here 10 μH is selected as the average value of the two solutions. Thanks to the high SRF of the inductor L_{2a}, the DF can be improved at high frequencies. Compared to the sectionalized windings that require advanced manufacturing techniques, this approach achieves a tradeoff between compact LISN volume and DF. The measured impedance and the fitted parameters of the circuit model for this additional inductor are shown in Fig. 11(a) and Table V. Thanks to L_{2a}, the DF is raised to above 60 dB from 5 MHz onwards (see the green curve in Fig. 12(b)), whereas in the original design, the DF gradually decreases to around 40 dB by 30 MHz (see the black curve in Fig. 12(b)). Although there is a resonance valley around 5.4 MHz due to the resonance between the inductance of L_{2a} and parasitic capacitance of L_2, the overall DF is above 40 dB after the compensation. It is worth mentioning that above 10 MHz, also mutual coupling between components, as well as the measurement setup, can play a role in the high-frequency behavior, although these effects were not considered in the equivalent circuit model for the sake of simplicity.

B. LISN Prototype and Experimental Assessment

The fabricated two-phase LISN prototype and its circuit diagram are presented in Fig. 13 and Fig. 14, respectively. The layout in Fig. 13 aims at reducing component coupling by increasing distance and changing orientations.

The LISN impedance is measured under various mains conditions using an impedance analyzer in the setup shown

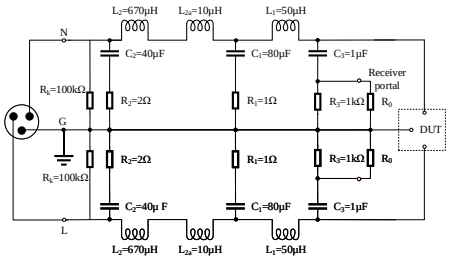

Fig. 14. Principle diagram of the two-phase LISN prototype.

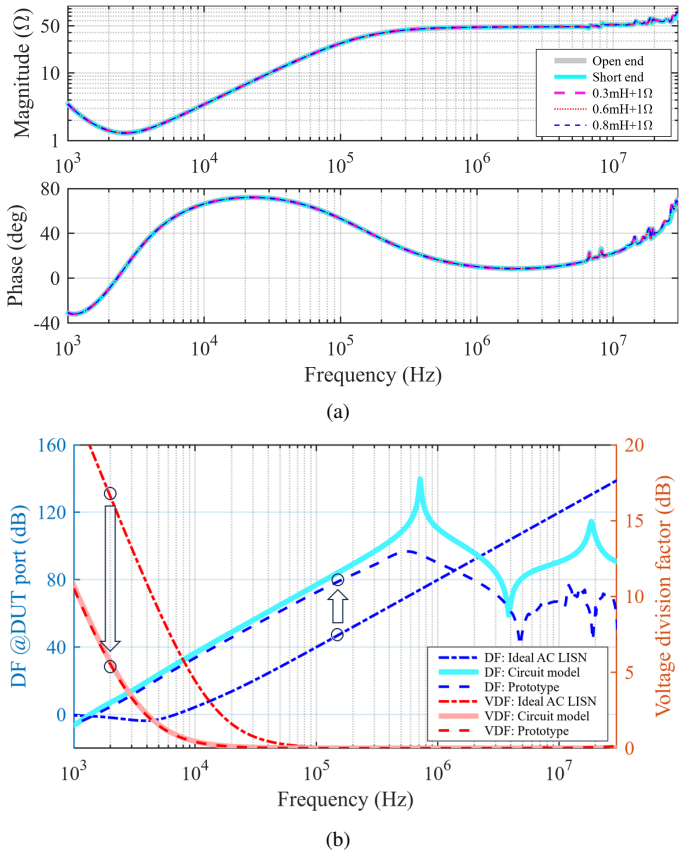

Fig. 15. Characteristics of LISN prototype of (a) LISN impedance under different mains conditions and (b) DF and VDF compared with the standard AC LISN.

in Fig. 14. Five conditions are selected, including open-end, short-end, and three different sets of RL components as dummy mains impedances. The comparisons reveal that the LISN impedance remains stable starting from 1 kHz. However, above 10 MHz, both the magnitude and phase exhibit some resonances attributed to the parasitic effects. Compared with the standard AC LISN in Fig. 2(a), the proposed LISN prototype significantly stabilizes the impedance at low frequencies.

The VDF of the LISN prototype is measured according to the standard setups specified in CISPR 16-1-2. The measurement results are compared versus theoretical predictions and the ideal standard AC LISN in Fig. 15(b). The comparison of VDF shows a good agreement between the prototype and the theoretical design. In comparison to the standard AC LISN, the proposed LISN exhibits a significant reduction in VDF at low frequencies. For instance, at 2 kHz, the VDF of the prototype is 5.5 dB, while for the ideal standard AC LISN it is 16.6 dB. The DF of the LISN prototype is measured between the mains and the DUT port, which agrees with the theoretical design at low frequencies and shows a significant increase compared to the standard AC LISN. The DF deviations between measurement and theoretical design in the circuit model is due to the fact that the circuit model neglects the influence of the mutual coupling between components, the connecting wires and layout, which actually play a role in DF reduction in the prototype.

VI. Conclusion

The manuscript has presented the design of a new LISN, suitable for CE measurement starting from 2 kHz. To this end, limitations of the available LISNs designed according to the current standards were firstly investigated, with the objective to identify the parameters to be optimized. The design methodology, exploiting a multi-objective optimization approach, focuses on improving LISN's characteristics at low frequencies (starting from 2 kHz) yet retaining the desired frequency behavior in the standard frequency range (9 kHz to 30 MHz). Various aspects, like tolerances in actual component values as well as not ideal behavior of the involved components, are considered for assuring the desired performance of the LISN prototype. Experimental results confirms that the manufactured LISN prototype outperforms the standard LISN in terms of frequency characteristics, thus allowing the measurement of conducted emissions starting from 2 kHz.

Acknowledgment

The authors would like to thank Matthew Cooper with the Power Electronics and Machines Control Department, University of Nottingham, for fabrication support.

References

[1] J. Luszcz and R. Smolenski, "Low frequency conducted emissions of grid connected static converters," *IEEE Electromagn. Compat. Mag.*, vol. 4, no. 1, pp. 86–94, Apr. 2015.

[2] F. Leferink, "Conducted interference, challenges and interference cases," *IEEE Electromagn. Compat. Mag.*, vol. 4, no. 1, pp. 78–85, Mar. 2015.

[3] *Signalling on low voltage electrical installations in the frequency range 3 kHz to 148.5 kHz*, Std. CENELEC 50 065-1, 2001.

[4] D. Ritzmann *et al.*, "Comparison of measurement methods for 2–150 kHz conducted emissions in power networks," *IEEE Trans. Instrum. Meas.*, vol. 70, pp. 1–10, Nov. 2020.

[5] V. Khokhlov, J. Meyer, A. Grevener, T. Busatto, and S. Rönnberg, "Comparison of measurement methods for the frequency range 2–150 kHz (supraharmonics) based on the present standards framework," *IEEE Access*, vol. 8, pp. 77 618–77 630, Apr. 2020.

[6] *Specification for radio disturbance and immunity measuring apparatus and methods - Part 1-2: Radio disturbance and immunity measuring apparatus - Coupling devices for conducted disturbance measurements*, Std. CISPR16-1-2, 2014.

[7] R. Amjadifard, M. T. Bina, H. Khaloozadeh, and F. Bagheroskouei, "Proposing an improved DC LISN for measuring conducted EMI noise," *IEEE Trans. on Electromagn. Compat.*, vol. 63, no. 3, pp. 752–761, Jun. 2021.

[8] I. Grobler and M. Gitau, "Low cost power lead extended pre-compliance conducted EMI measurement setup and diagnostics with compact LISN," in *Proc. IEEE ECCE Asia Downunder*, 2013, pp. 1144–1149.

[9] Y. Sun, X. Zhang, W. Chien, C. H. Sun, and C. C. Chiu, "Development of a new line impedance stabilization network system," in *Proc. 3rd IEEE Int. Symp. Microw., Antenna, Propag. EMC Technol. Wireless Commun.*, Beijing, China, Oct. 2009, pp. 363–366.
[10] D. Sakulhirirak, V. Tarateeraseth, W. K. Ngern, and N. Yoothanom, "A new simultaneous conducted electromagnetic interference measuring and testing device," in *Proc. Asia-Pacific Symp. Electromagn. Compat. 19th Int. Zurich Symp. Electromagn. Compat.*, Singapore, May 2008, pp. 606–609.
[11] A. Mariscotti, L. Sandrolini, and G. Pasini, "Variability caused by setup and operating conditions for conducted EMI of switched mode power supplies over the 2–1000 kHz interval," *IEEE Trans. Instrum. Meas.*, vol. 71, pp. 1–9, Mar. 2022.
[12] A. Khilnani, L. Wan, M. Sumner, D. Thomas, A. Hamid, and F. Grassi, "Conducted emissions measurements in DC grids: Issues in applying existing lisn topologies and possible solutions," in *Proc. IEEE 15th Int. Conf. Compat., Power Electron. Power Eng.*, Jul. 2021, pp. 1–6.
[13] L. Wan *et al.*, "Limitations in applying the existing LISN topologies for low frequency conducted emission measurements and possible solution," in *Proc. Asia-Pacific Int. Symp. Electromagn. Compat.*, Sept. 2021, pp. 1–4.
[14] S. Nitta, "Roles and problems of lisn in noise measurement," *IEICE Trans. Commun.*, vol. 78, no. 2, pp. 109–119, Feb. 1995.
[15] R. Stiegler *et al.*, "Survey of network impedance in the frequency range 2-9 kHz in public low voltage networks in AT/CH/CZ/GE," in *Proc. 25th Int. Conf. Electr. Distrib.*, Jun. 2019, pp. 3–6.
[16] K. Miettinen, *Nonlinear multiobjective optimization,* vol. 12. New York, NY, USA: Springer, 2012.
[17] *Matlab Optimization Toolbox (R2022b)*, Accessed: Sept. 2022. [Online]. Available: https://www.mathworks.com
[18] H. Nagaoka, "The inductance coefficients of solenoids," *J. College Sci.*, vol. 27, pp. 1–33, 1909.
[19] R. Medhurst, "HF resistance and self-capacitance of single-layer solenoids," *Wireless Eng.*, vol. 24, pp. 35–43, Feb. 1947.
[20] H. A. Wheeler, "Simple inductance formulas for radio coils," *Proc. Inst. Radio Eng.*, vol. 16, no. 10, pp. 1398–1400, Oct. 1928.
[21] H. Zuhrt, "Simple approximate formulas for the self capacitance of multi-layer coils," *Elekrotech. Zeitschrift*, vol. 55, pp. 662–665, 1934.

Lu Wan (Member, IEEE) received the double M.Sc. degrees in electrical engineering from Xi'an Jiaotong University, Xi'an, China, and Politecnico di Milano, Milan, Italy, in 2017, and the joint Ph.D degree (summa cum laude) in electrical engineering from Politecnico di Milano and the University of Craiova, Craiova, Romania, in 2023.

He is currently a Scientist with Hitachi Energy Research, Switzerland. From 2017 to 2019, he was an Assistant Researcher with the Electric Power Research Institute, China Southern Power Grid. In 2023, he was with the Energy Department, Aalborg University, as a Postdoctoral Researcher. His research interests include electromagnetic design and analysis of power electronic equipment, and modeling of complex and multiscale systems.

Arun D. Khilnani (Member, IEEE) received the bachelor's degree in Electrical Engineering from the University of Mumbai, India, in 2009, the master's degree in electric power engineering from Chalmers University of Technology, Gothenburg, Sweden, in 2019, and the Ph.D.degree in electrical and electronic engineering from the University of Nottingham, Nottingham, U.K., in 2024. From 2009 to 2015, he holds more than six years of professional experience as an Electrical Engineer. He is currently a Research Fellow with the University of Nottingham. His research interests are focused on electromagnetic compatibility and power electronics.

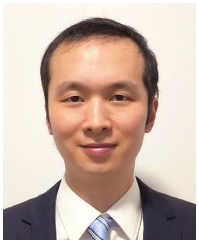

Xinglong Wu (Senior Member, IEEE) received the double M.Sc. degrees from Xi'an Jiaotong University, Xi'an, China and Politecnico di Milano, Milan, Italy, in 2015, and the Ph.D. degree (cum laude) from Politecnico di Milano, in 2019, all in electrical engineering.

He is currently an Assistant Professor with the Department of Electronics, Information and Bioengineering, Politecnico di Milano. In March 2017 and June 2017, he was a Visiting Scientist with the Electromagnetics Group, Department of Information Technology, Ghent University, Belgium. From 2019 to 2020, he was a Postdoctoral Research Fellow with Politecnico di Milano. His research interests include distributed parameter circuit modeling, statistical techniques for electromagnetic compatibility (EMC), experimental procedures and setups for EMC testing, power electronics EMC, and system-level EMC.

Dr. Wu was the recipient of the International Union of Radio Science (URSI) Young Scientist Award from the 2020 URSI General Assembly and Scientific Symposium.

Xiaokang Liu (Senior Member, IEEE) received the double M.Sc. degrees in electrical engineering from Xi'an Jiaotong University, Xi'an, China, and Politecnico di Milano, Milan, Italy, in 2016, and the Ph.D. degree in electrical engineering from Politecnico di Milano, in 2021.

From 2021 to 2024, he was an Assistant Professor with the Department of Electronics, Information, and Bioengineering, Politecnico di Milano. He is currently a Disgtinguished Research Fellow with the College of Electrical Engineering, Sichuan University, Chengdu, China. His research interests include electromagnetic compatibility, power electronics, and signal integrity.

Dr. Liu was a recipient of the International Union of Radio Science Young Scientist Award, in 2021, and the 2021 Richard B. Schulz Best EMC Transactions Paper Award.

Sergio A. Pignari (Fellow, IEEE) received the Laurea (M.Sc.) and Ph.D. degrees in electronic engineering from Politecnico di Torino, Turin, Italy, in 1988 and 1993, respectively. From 1991 to 1998, he was an Assistant Professor with the Department of Electronics, Politecnico di Torino. In 1998, he joined Politecnico di Milano, Milan, Italy, where he is currently a Full Professor of circuit theory and electromagnetic compatibility (EMC) with the Department of Electronics, Information, and Bioengineering. He served as the Chair for the B.Sc. and M.Sc. Study Programmes in electrical engineering, term (2015–2020). He is the author or coauthor of more than 220 papers published in international journals and conference proceedings. His research interests are in the field of EMC and include field-to-wire coupling and crosstalk, conducted immunity and emissions in multi-wire structures, statistical techniques for EMC prediction, and experimental procedures and setups for EMC testing. His research activity is mainly related to aerospace, automotive, energy, and railway industry sectors.

Dr. Pignari was a co-recipient of the 2005, 2016, and 2021 IEEE EMC Society Transactions Prize Paper Award, and received the IEEE EMC Society Technical Achievement Award in 2011. He is currently serving as an Associate Editor for the IEEE TRANSACTIONS ON ELECTRO- MAGNETIC COMPATIBILITY. From 2010 to 2015, he served as the IEEE EMC Society Chapter Coordinator. From 2007 to 2009, he was the Chair of the IEEE Italy Section EMC Society Chapter. He served as the Italian URSI Officer for Commission E (Electromagnetic Noise and Interference), term (2015–2018). He has been the Technical Program Chair of the ESA Workshop on Aerospace EMC since 2009, and a member of the Technical Program Committee of the Asia Pacific Int. Symp. on EMC since 2010.

David W.P. Thomas (Senior Member, IEEE) received the B.Sc. degree in physics from Imperial College, London, U.K., in 1981, the M.Phil. degree in space physics from Sheffield University, Sheffield, U.K., in 1984, and the Ph.D. degree in electrical engineering from Nottingham University, Nottingham, U.K., in 1990.

He is currently a Professor of electromagnetics applications with the George Green Institute for Electromagnetics Research, The University of Nottingham, Nottingham, U.K. His research interests include electromagnetic compatibility, electromagnetic simulation, power system transients, and power system protection.

Prof. Thomas is a member of CIGRE and Convenor for Joint Working Group C4.31 EMC between communication circuits and power systems, Chair of COST Action IC 1407 "Advanced characterization and classification of radiated emissions in densely integrated technologies," a member of several conference committees, and the EMC Europe International Steering Committee.

Mark Sumner (Senior Member, IEEE) (Senior Member, IEEE) received the B.Eng. degree in electrical and electronic engineering from the University of Leeds in 1986, and the Ph.D. degree in induction motor drives from the University of Nottingham, U.K., in 1990.

He was with Rolls Royce Ltd., U.K. He was also a Research Assistant and a Lecturer in October 1992. He is currently a Professor of Electrical Energy Systems with the Power Electronics, Machines and Control Group, University of Nottingham. His research interests include control of power electronic systems, including sensorless motor drives, diagnostics and prognostics for drive systems, power electronics for enhanced power quality, and novel power system fault location strategies.

Flavia Grassi (Senior Member, IEEE) received the Laurea (M.Sc.) and Ph.D. degrees in electrical engineering from Politecnico di Milano, Milan, Italy, in 2002 and 2006, respectively.

She is currently a Full Professor in the Department of Electronics, Information and Bioengineering, Politecnico di Milano. From 2008 to 2009, she was with the European Space Agency (ESA), ESA/ESTEC, The Netherlands, as a Research Fellow. Her research interests include: Theoretical and experimental characterization of EM interference via lumped and distributed circuit modeling; characterization and development of measurement procedures and setups for EMC assessment of avionic, automotive, and power systems; statistical techniques, EMC and coexistence issues in power systems.

Dr. Grassi received the International Union of Radio Science (URSI) Young Scientist Award in 2008, and the IEEE Young Scientist Award at the 2016 Asia-Pacific Int. Symposium on EMC (APEMC), the IEEE EMC Society 2016 and 2021 Transactions Prize Paper Award, and the Best Symposium Paper Award at the 2015 and 2018 APEMC.